A Study Using Relativistic Hydrodynamics for Ultrarelativistic Heavy-Ion Collisions: The Quark-Gluon-Plasma to Hadron Phase Transition and LHC Predictions

A Senior Honors Thesis

Presented in Partial Fulfillment of the Requirements for graduation with research distinction in Physics in the undergraduate colleges of The Ohio State University

By

Gregory M. Kestin

The Ohio State University

May 2008

Project Advisor: Professor Ulrich Heinz, Department of Physics

ABSTRACT

A brief introduction into the study of quark-gluon plasma (QGP) created in heavy-ion collisions is given. Subsequently, results are reported from studies of several specific topics using relativistic hydrodynamics to model the evolution of QGP created in such collisions.

INTRODUCTION

This thesis first discusses background and motivation for studying relativistic heavy-ion collisions. It then reviews our work corroborating the quark-gluon plasma to hadron phase transition theory for chemical decoupling. Lastly, a number of hydrodynamic predictions are presented for collisions that range from AGS to LHC energies.

BACKGROUND

Quark-Gluon Plasma at the Beginning of Time

Immediately after the Big Bang, no molecules, atoms, or even nucleons existed; all matter was smashed together in an immensely dense material known as Quark-Gluon Plasma (QGP). After a few microseconds all the quarks and gluons that comprised the primordial QGP settled into nucleons and other stable particles. Now, billions of years later, the density of energy in the universe has decreased enough for these particles to organize themselves into matter as we know it [1].

Studying QGP on Earth

For two decades, particle accelerators around the world have been colliding atomic nuclei at immense velocities to discover what interacting nuclei do at such energetic impacts. Research related to such experiments has deduced that QGP is created in these collisions. The Relativistic Heavy-Ion Collider (RHIC) is one such accelerator. We use the data from a particular experiment attached to RHIC, called the STAR experiment. We mainly study the collisions of gold (Au) nuclei. The gold nuclei do not always perfectly overlap at impact; when there is a small overlap the collision is called a peripheral collision, and when the nuclei greatly overlap, the collision is called a central collision. The overlap is measured by a parameter called the impact parameter (b), which is the shortest distance between the centers of the two nuclei. For collision involving two gold nuclei, the impact parameter ranges from 0 to 14 femtometers (1 femtometer$= 1 \times 10^{-15}$ meters).

Within a time span of no more than 20 fm/c ($\approx 6.7{\times}10^{-23}$ seconds!) after the nuclei collide, the QGP in the collision heats up, expands, hadronizes (i.e. the color-charged quarks and gluons combine into hadrons, color-neutral strongly interacting particles), and finally breaks up. The hadrons continue to move outward, and their properties are measured by detectors at the experimental sites.

MODELING QGP

In 1992, it became evident that relativistic hydrodynamics gives a fair representation of the evolution of the QGP created in relativistic nuclear collisions [2]. More recent data from RHIC have shown that at higher energies the hydrodynamic model becomes even more accurate and provides a quantitative description of the bulk of experimental data on hadron production [3]. The hydrodynamic model has been used to create a computer program, AZHYDRO [4], that simulates relativistic

heavy-ion collisions and the evolution of the QGP generated in the collisions. The program uses a (2+1)-dimensional model for the evolution of the QGP; that is, we look at the evolution of the plasma in the x-y plane at midrapidity for a finite number of steps in proper time.

THE QGP-HADRON PHASE TRANSITION

This section reviews our work corroborating the QGP-hadron phase transition theory for chemical decoupling. We use the above model for the evolution of the QGP. We find that any kinetic decoupling process leads to a collision centrality dependence of the decoupling temperature. Since STAR data show that chemical decoupling temperature does not exhibit centrality dependence, we conclude that chemical decoupling cannot be understood as a kinetic process, but must be driven by a phase transition.

Two Processes During Evolution of the System

There are two important processes that occur during the evolution of the system of matter created in a heavy-ion collision. One is called chemical decoupling, and the other is called kinetic freeze-out.

1. Chemical decoupling is the process by which the changes in the chemical composition (i.e., the relative abundances of the different hadron species) cease.

   The STAR experiment at RHIC has determined the average temperature (T_{Chem}) at chemical decoupling, by analyzing the final abundances of different hadron species in collisions with various impact parameters [5]. The experimental results show that chemical decoupling always occurs at an approximately constant temperature (see STAR data on Figure 1). Other experiments have shown that chemical decoupling occurs at about the same temperature in proton-proton collisions. This suggests that at chemical decoupling there may be a phase transition from a quark-gluon plasma (QGP) to a hadron gas as has been predicted by Lattice Quantum-Chromodynamics [6]; this phase change happens at a critical temperature T_C.

2. Kinetic freeze-out is the process by which hadron momenta change for the last time.

   The STAR experiment at RHIC has determined the average temperature (T_{Kin}) at kinetic freeze-out, by analyzing the shape of the hadronic velocity distributions for collisions with various impact parameters [5]. The kinetic freeze-out temperature is found to change with collision centrality (see STAR data in Figure 2); it thus seems to be sensitive to the dynamics of the expanding system of particles.

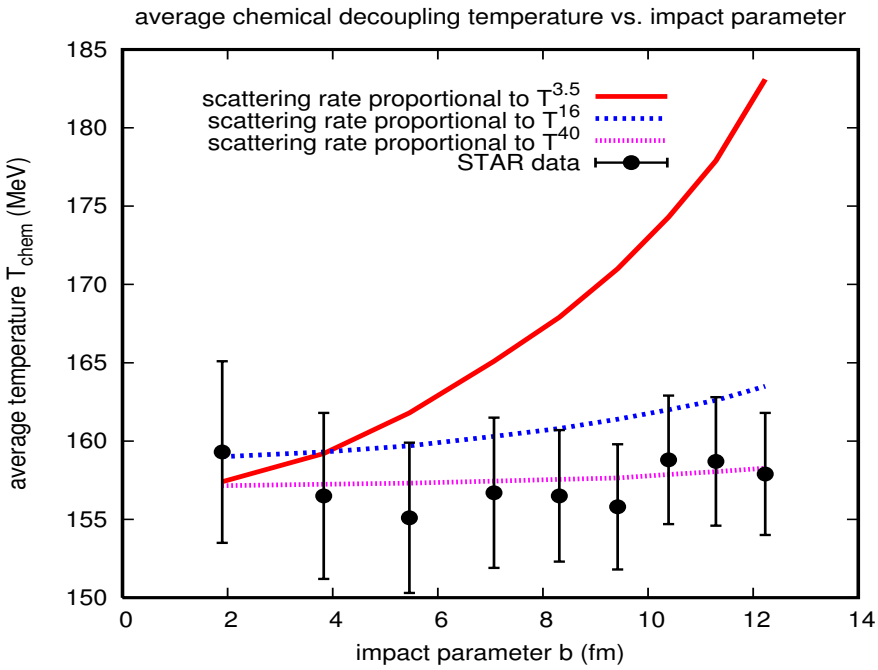

FIG. 1: Average chemical decoupling temperature as a function of impact parameter.

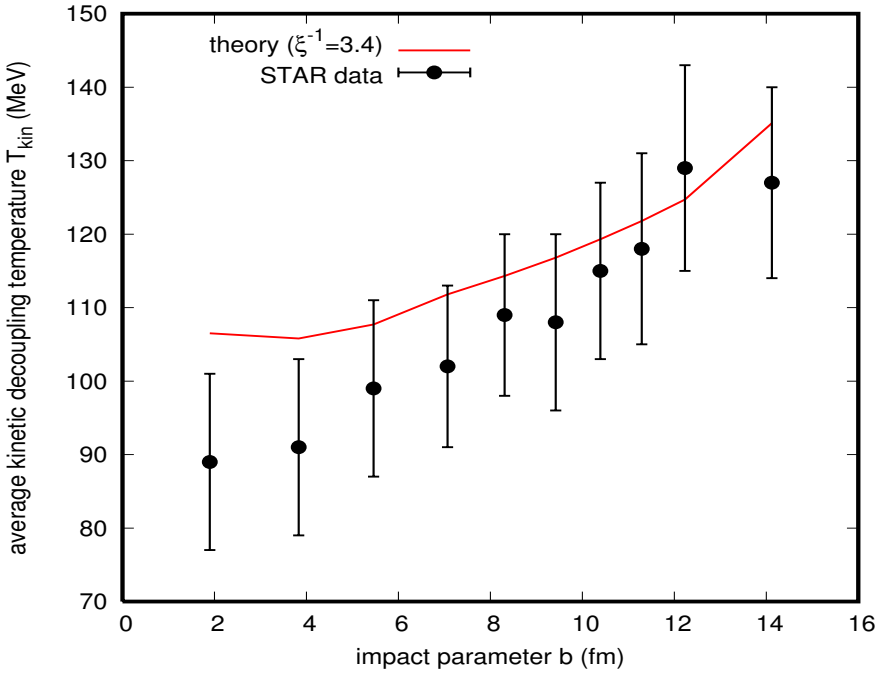

FIG. 2: Average kinetic freeze-out temperature as a function of impact parameter.

Two Theories for Describing Chemical Decoupling

1. Theory 1

   QGP converts to hadrons at $T_C > T_{Chem}$, and T_{Chem} is interpreted [7] as reflecting the kinetic transition from highly dense hadrons undergoing multi-particle interactions (which change the

chemical composition of the particles) to a more dilute system of hadrons undergoing only elastic scatterings (which just cause momentum transfer). One problem with this theory is that any kinetic process should depend on the expansion dynamics of the system, but no such dependence is observed for T_{Chem}. That is, we expect T_{Chem} to be different for different impact parameters, since more peripheral collisions will have different expansion dynamics. This is in contrast with what is seen in Figure 1: T_{Chem} is constant over all impact parameters. Also, this theory begs the question: Why is T_{Chem} so close to the predicted T_C?

2. Theory 2

   Chemical decoupling is driven by the QGP-to-hadron phase transition at critical temperature T_C, analogous to the phase change of water to ice at 0 degrees Celsius, and T_{Chem} and T_C are actually identical. This theory provides natural answers to problem with Theory 1.

Technique

We will first assume that Theory 1 models the evolution of the system created in the nuclear collisions, and that both chemical decoupling and kinetic freeze-out are described as kinetic processes. So, we will model both by using appropriate kinetic decoupling criteria. A kinetic decoupling criterion means that decoupling occurs when the rate at which the system is expanding becomes significantly greater than the rate of scattering of the particles amongst each other.

The kinetic decoupling criterion employed by us determines the proposed decoupling surface by finding all the points with a particular, chosen ratio of the scattering rate $(1/\tau_{scatt})$ to the expansion rate $(1/\tau_{exp})$; these points compose the proposed decoupling surface. Therefore, the expression used to determine the decoupling surfaces is: $(1/\tau_{scatt}) = C/\tau_{exp}$, where C is a parameter of order unity which is adjusted to reproduce the observed decoupling temperatures in the most central collisions.

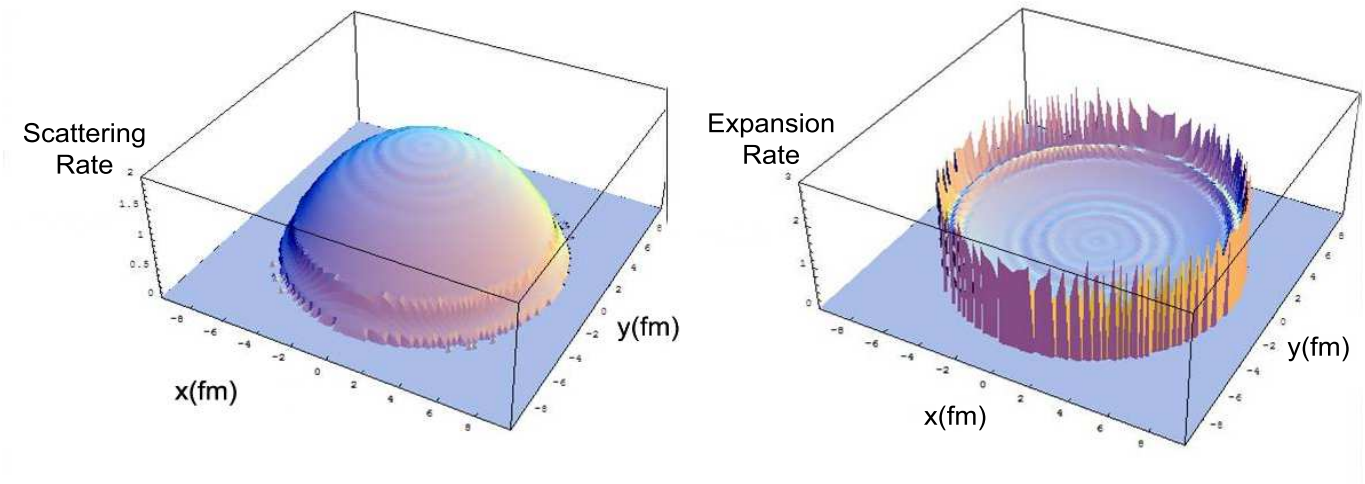

FIG. 3: Visualization of expansion and scattering rate at a fixed time in a central collision. If one imagines these two figures overlapped, then the intersection of the surfaces (if $C = 1$) gives the (x, y) coordinates at which the system decouples in this model for kinetic decoupling.

The expansion rate (which is computed from the hydrodynamic output for the transverse flow velocity $\boldsymbol{v}_\perp(x)$ and $\gamma_\perp = (1 + v_\perp^2)^{-1/2}$) is found to be the following expression:

$$\frac{1}{\tau_{scatt}} = \partial \cdot u = \gamma_\perp \left(\frac{1}{\tau} + \boldsymbol{\nabla}_\perp \cdot \boldsymbol{v}_\perp \right) + (\partial_\tau + \boldsymbol{v}_\perp \cdot \boldsymbol{\nabla}_\perp)\, \gamma_\perp. \tag{1}$$

(Here $\perp$ indicates the directions x, y perpendicular to the beam direction.) One sees that the expansion rate depends on the expansion flow velocity of the system created in the collision.

Since the system is found to be replete with pions, we have used a parameterization of the scattering rate of pions as a function of temperature in a pion-kaon-nucleon gas [9]:

$$\frac{1}{\tau^{\pi}_{scatt}} = \left(59.5\,\mathrm{fm}^{-1}\right)\left(\frac{T}{1\,\mathrm{GeV}}\right)^{3.45}. \tag{2}$$

Results

With this kinetic decoupling criterion, we have computed the average temperatures on the chemical and kinetic freeze-out surfaces for collisions with different impact parameters. The solid line in figure 2 shows the resulting impact parameter dependence of the average kinetic freeze-out temperature (here $C_{kin} = 0.3$). One sees that the computed impact parameter dependence nicely reproduces the experimental data from the STAR experiment.

The solid line in figure 1 shows the impact parameter dependence of the average chemical decoupling temperature predicted by Theory 1 (here $C_{chem} = 1.05$). The predicted strong dependence on collision centrality does not agree with the experimental data from the STAR experiment.

Discussion

The kinetic decoupling criterion correctly reproduces the experimental tendency for higher freeze-out temperatures in more peripheral collisions. The agreement is not perfect, but it is known that ideal fluid dynamics has problems in very peripheral collisions in that it also overestimates the measured anisotropies (see below) of the final system of particles there. In view of this, the qualitative agreement with the data in Figure 1 is actually quite impressive. This figure shows that in nature kinetic freeze-out (i.e., the final decoupling of the velocity distributions of the hadrons) indeed occurs when the expansion rate exceeds the scattering rate, as suggested in [2].

On the other hand, the average temperature of chemical decoupling is found experimentally to be constant over all impact parameters. Hence, it cannot be determined similarly by the competition between expansion and scattering rates. This invalidates the explanation for chemical decoupling given by Theory 1 [7].

In order for a kinetic decoupling criterion to accurately model chemical decoupling it would have to yield a constant temperature for all impact parameters. This requires the scattering rate to be a very steep function of temperature. The known elastic 2-body scattering rate for pions in a pion-kaon-nucleon gas, parameterized by equation (2), is proportional to $\mathrm{T}^{3.45}$. If chemical decoupling were similarly controlled by *inelastic* 2-body collisions, the chemical reaction rate should have a similar T-dependence. As we see from Figure 1, however, such a T-dependence yields an increase of chemical decoupling temperature with impact parameter, contrary to what is seen in experiment.

Figure 1 shows the chemical decoupling temperature resulting from the kinetic decoupling criterion for 3 different assumed temperature dependences of the scattering rate. We see that the agreement with the experimental data improves if the temperature dependence of the scattering rate becomes steeper (i.e. for larger exponents). We notice, however, that even a scattering rate proportional to T^{16} still creates an impact parameter dependence of T_{Chem} that is larger than experimentally observed. It seems that an almost infinitely steep scattering rate is required to maintain a constant chemical decoupling temperature at all impact parameters.

Any phase transition occurs at one specific temperature, and therefore involves microscopic processes that have an infinitely steep dependence on temperature. Thus, the quark-gluon plasma-hadron phase transition predicted by lattice quantum-chromodynamics is an ideal process to drive chemical decoupling in relativistic heavy-ion collisions. Therefore, the model presented by Theory 2 is indeed consistent with the experimental data found at RHIC.

Conclusion

The description of chemical decoupling as a kinetic process involving inelastic scatterings among hadrons (given by Theory 1) does not produce results consistent with the experimental data. The explanation of chemical decoupling as being driven by a QGP-hadron phase transition (given by Theory 2) is consistent with the experimental data.

AGS TO LHC PREDICTIONS

In this section we again use the (2+1)-dimensional hydrodynamic simulation program, but now we look at a few different trends for collisions whose energies range from AGS energies to LHC energies. Specifically we look at particle spectra, particular particle ratios, and elliptic flow v_2 at midrapidity. Elliptic flow v_2 provides a measure of momentum anisotropy of the system. We will look at both differential elliptic flow as a function of transverse momentum p_T, as well as p_T-integrated elliptic flow.

Procedure

To run the simulation we must initialize the program by providing the following parameters:

1. impact parameter b (explained in previous section)
2. initial proper time τ_0: this indicates the proper time after nuclear impact at which the simulation begins and hydrodynamics may be accurately employed.
3. initial net baryon number density $n_{B,0}$: net density of baryons at τ_0.
4. initial peak entropy density s_0: the highest local entropy density in central collisions at τ_0. This value is used to control the energy of the simulated collision.

We must also provide a criterium for kinetic freeze-out, for which we here choose for simplicity a constant decoupling temperature $T_{dec} = 130\,\mathrm{MeV}$. Implementing the kinetic decoupling criterium from the first part of this thesis is numerically involved and not necessary for the study to be presented in the following.

In order to initialize our simulations we must know the above initialization parameters. Here we will look at both central collisions ($b = 0$) and peripheral collisions with $b = 7\,\mathrm{fm}$ (whenever we are presenting elliptic flow in this paper, we are speaking of Au+Au collisions with $b = 7\,\mathrm{fm}$). τ_0 is chosen such that the uncertainty relation $T_0\tau_0 = \text{const.}$ is satisfied. $n_{B,0}$ is kept at a value of $0.44/\mathrm{fm}^3$, except at LHC energies where $n_{B,0}$ is set to 0. This reflects the decreasing ability of the nuclei, as their collision energy increases, to stop the valence quarks of the colliding nuclei in the midrapidity region. The net baryon number thus accumulates near beam rapidity, and the baryon/entropy ratio at midrapidity becomes smaller and smaller as the collisions become more and more energetic.

Finding the value for s_0 is more involved. Since we wish to look at collisions whose energies approach LHC energies, which has an unknown charged particle multiplicity and therefore an unknown initial peak entropy density ($dN_{Charged}/d\eta \propto s_0$), we must make some sort of extrapolation from known data. In Figure 4 data from experiments at the RHIC, SPS, and AGS accelerator complexes, as compiled in [8], are shown in a semi-logarithmic plot. We have fitted these data using a linear fit, giving the following relationship between collision energy and charged particle multiplicity:

$$\frac{dN_{Charged}}{d\eta} = 312.5 \times \log_{10}(\sqrt{s}) - 64.8 \tag{3}$$

The crosses in Figure 4, all of which lie on this trend line, indicate the charged particle multiplicity and s_0 used in hydrodynamic simulations. Now, with all initial conditions specified, we are ready to run the simulations.

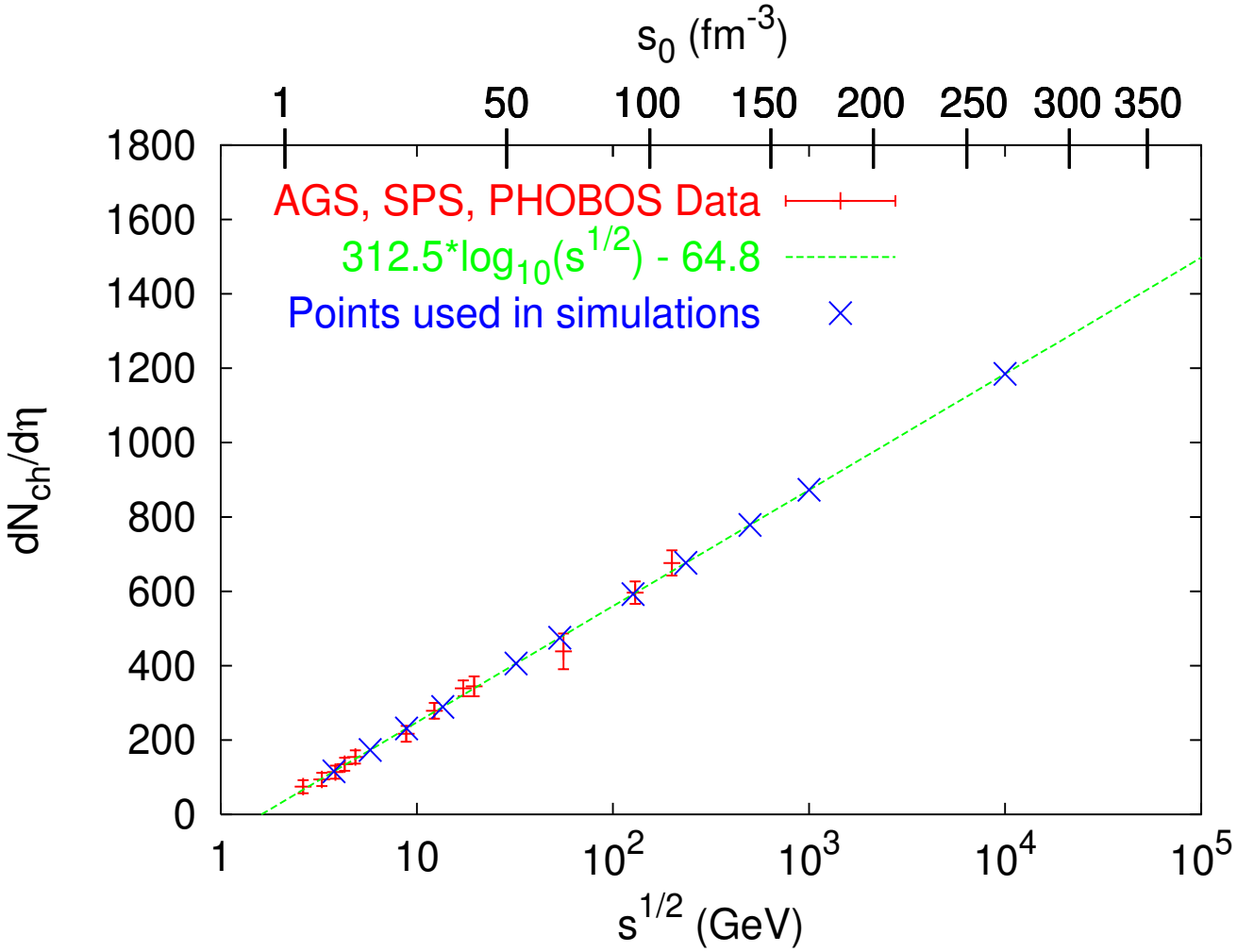

FIG. 4: Charged particle multiplicity as a function of center of mass energy $\sqrt{s}$ (lower horizontal axis) and s_0 (upper horizontal axis). The experimental data (red symbols), which can be found in [8], are for Au+Au and Pb+Pb collisions at RHIC, SPS, and AGS energies. Blue crosses indicate charged particle multiplicity and s_0 values used in our hydrodynamic simulations.

Radial Flow

Transverse momentum spectra from AGS to LHC energies

We have computed the p_T-spectra for thermally emitted π^+ mesons and protons (Figure 5). The left panels are expanded views of the low-p_T end of the spectra. We see that the π^+ spectra increase in magnitude as collision energy increases, reflecting the increasing total charged hadron multiplicity $dN_{Charged}/dy$. It is important to point out the flattening of the spectra with increasing collision energy: Because T_{dec} is held constant, this means that the radial flow increases with the collision energy.

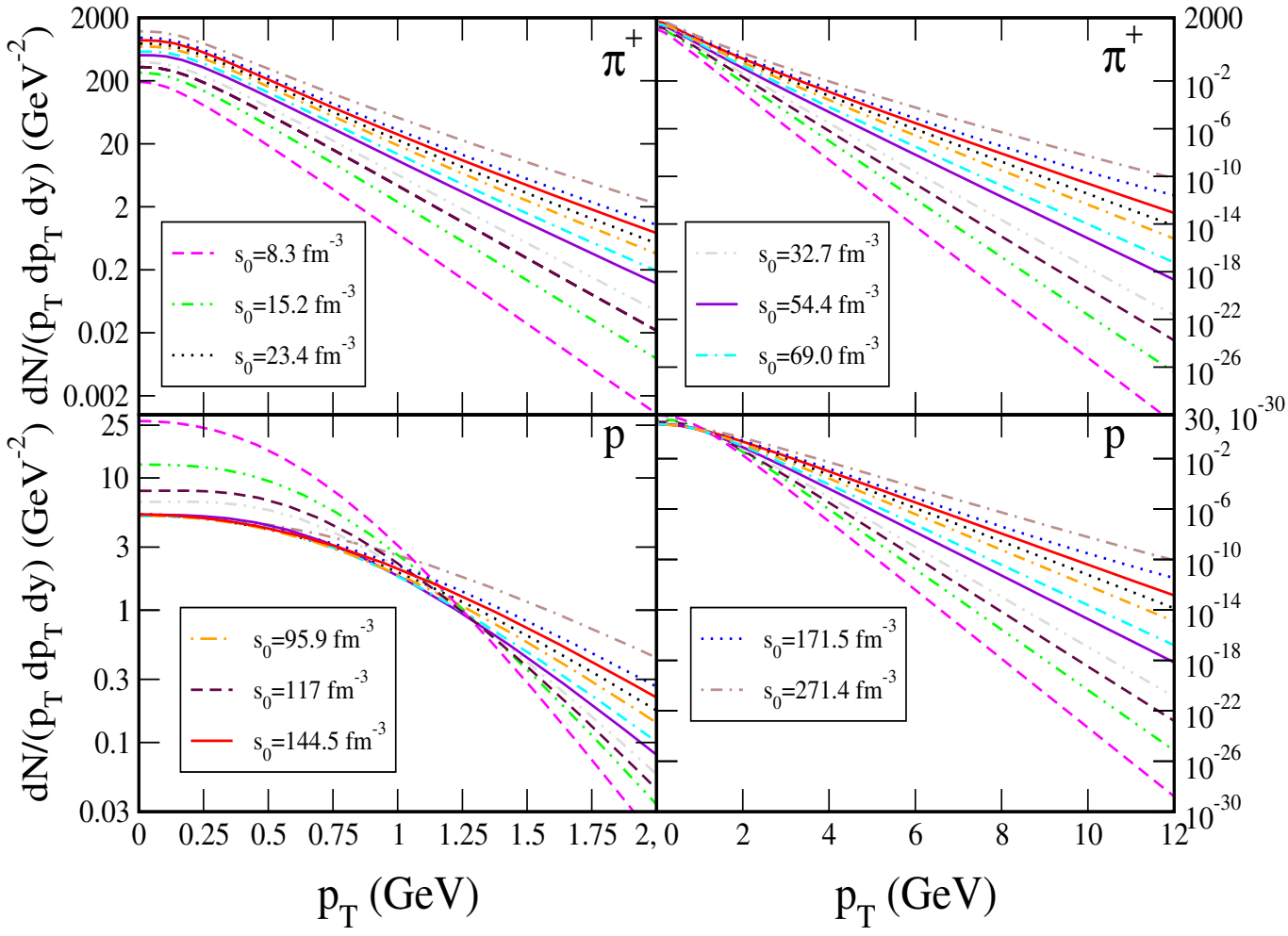

FIG. 5: π^+ (top panels) and proton (lower panels) spectra as a function of transverse momentum for central Au+Au collisions with various initial peak entropy densities s_0.

Looking at the behavior of the proton spectra we see something a little different. While the spectra similarly flatten out with an increase in collision energy indicating an increase in radial flow, the naive expectation with regard to the magnitude of the spectra at low p_T is not met. Rather than featuring yields that increase with collision energy at all values of p_T, as seen for the π^+, the proton spectra decrease at low p_T with higher collision energy. While the p_T-integrated proton levels may increase monotonically with collision energy, the low-p_T part of the spectra seems to decrease monotonically at any given low p_T. This is due to the large increase in radial flow; it moves the protons from low p_T to higher transverse momenta, flattening the spectra so much that the low-p_T

yield actually *decreases* below that seen in lower energy collisions. This occurs for the protons and not for pions because the p_T spectra flatten more dramatically for heavier particles.

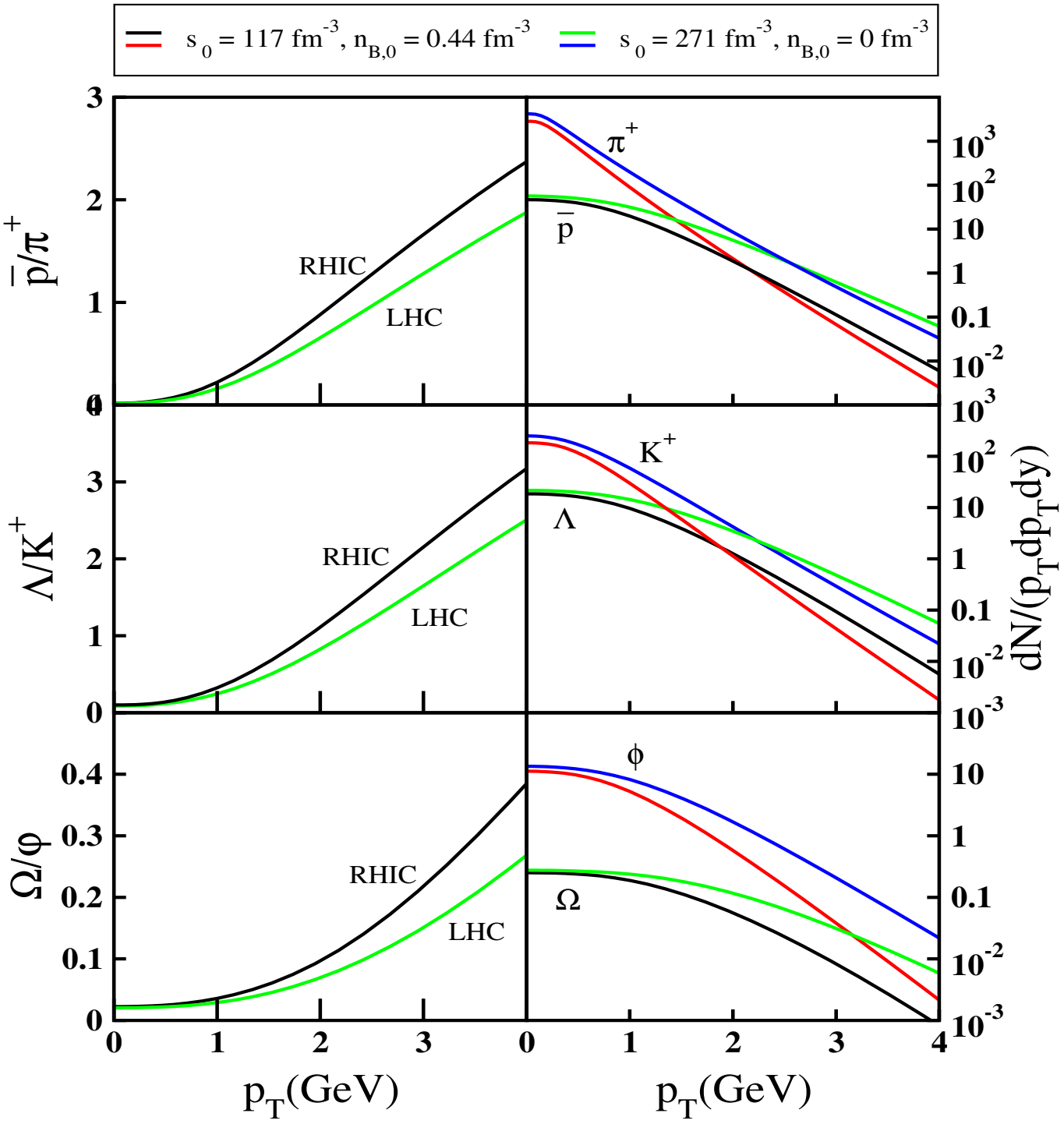

FIG. 6: Particle ratios as a function of transverse momentum (left). Particle ratios at RHIC ($s_0 = 117\,\mathrm{fm}^{-3}$) and LHC ($s_0 = 271\,\mathrm{fm}^{-3}$) energies as a function of transverse momentum (right). For central Au+Au collisions.

p_T- and m_T-dependent particle ratios: RHIC vs. LHC

Hydrodynamic flow, which leads to flatter p_T-spectra for heavy particles, is a key contributor to the observed strong rise of the $\bar{p}/\pi$ and Λ/K ratios at low p_T at RHIC [3]. Figure 6 shows that this

rise is predicted to be slower at LHC than at RHIC (left column) since *all* spectra are flatter at LHC due to increased radial flow (right column) while their asymptotic ratios at $p_T \to \infty$ (given by their fugacity and spin degeneracy ratios [3]) remain similar.

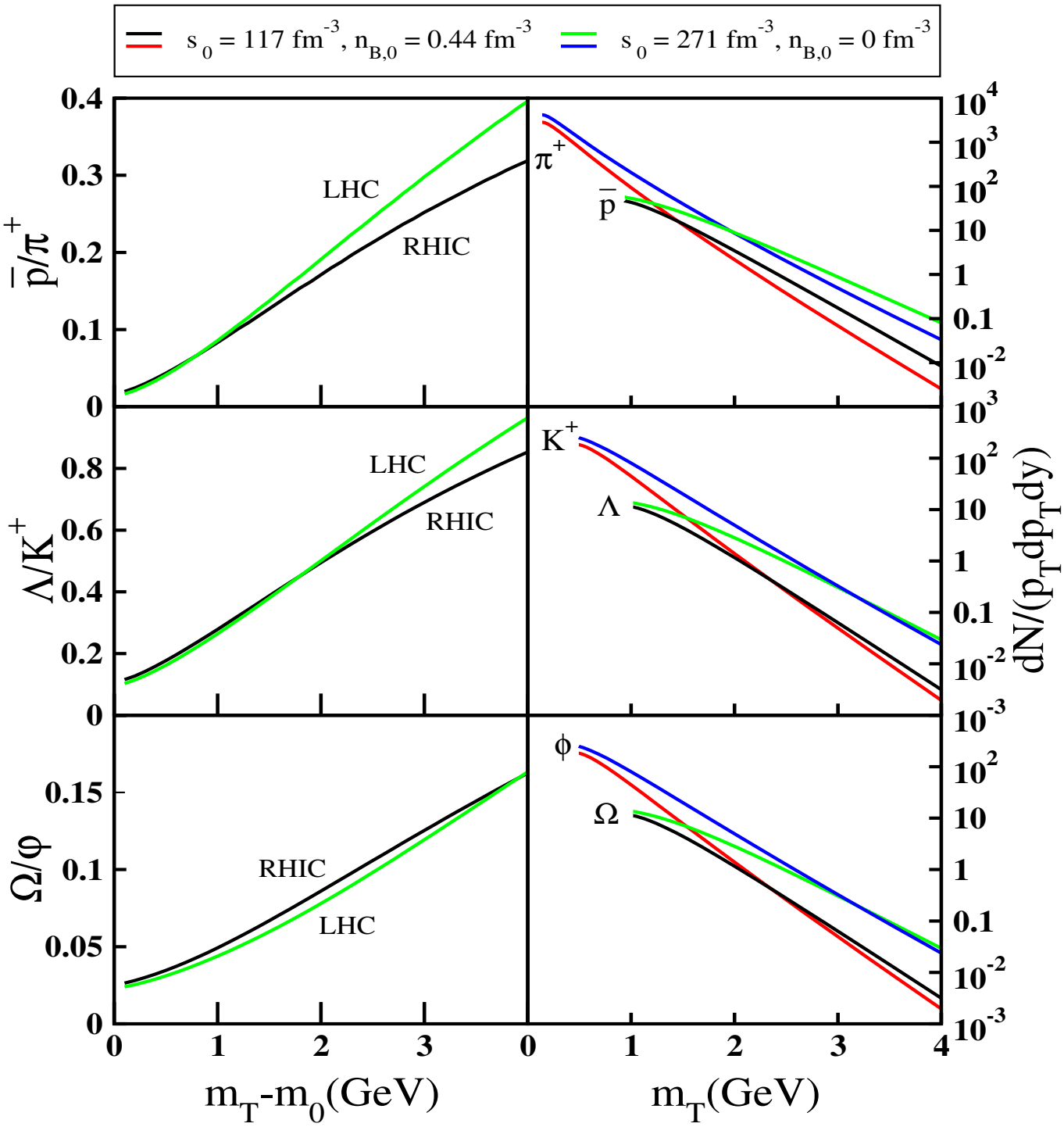

FIG. 7: Particle ratios as a function of transverse kinetic energy (left). Particle ratios at RHIC ($s_0 = 117\,\mathrm{fm}^{-3}$) and LHC ($s_0 = 271\,\mathrm{fm}^{-3}$) energies as a function of transverse mass (right). For central Au+Au collisions.

Figure 7 is the same as Figure 6, but now the spectra (right) are a function of transverse mass m_T, and the particle ratios are a function of transverse kinetic energy $m_T - m_0$. There are other reasons

(e.g. "baryon junctions" [10]) predicted for these ratios to rise as a funtion of $m_T - m_0$, but my work shows that they rise also simply due to radial flow which gives flatter spectra for the heavy baryons ($\bar{p}$, Λ, and Ω) than the much lighter mesons (π, K, and ϕ). Figure 7 establishes hydrodynamic benchmarks for the LHC, so that only observed rises much faster than these benchmarks should be claimed to be signatures for new physics.

Elliptic Flow

While ideal fluid dynamics begins to break down below RHIC energies, due to viscous effects in the late hadronic stage which persist even at RHIC [11], its validity is expected to improve at the LHC where the elliptic flow saturates in the quark-gluon plasma (QGP) stage, and effects from late hadronic viscosity become negligible [12]. Early QGP viscous effects seem small at RHIC [3, 11], and recent results from Lattice QCD indicate little change of its specific shear viscosity η/s from RHIC to LHC [13]. The following *ideal fluid* dynamical predictions for soft ($p_T \lesssim 2{-}3\,\mathrm{GeV}/c$) hadron production in ($A{\approx}200$)+($A{\approx}200$) collisions at the LHC should thus be robust.

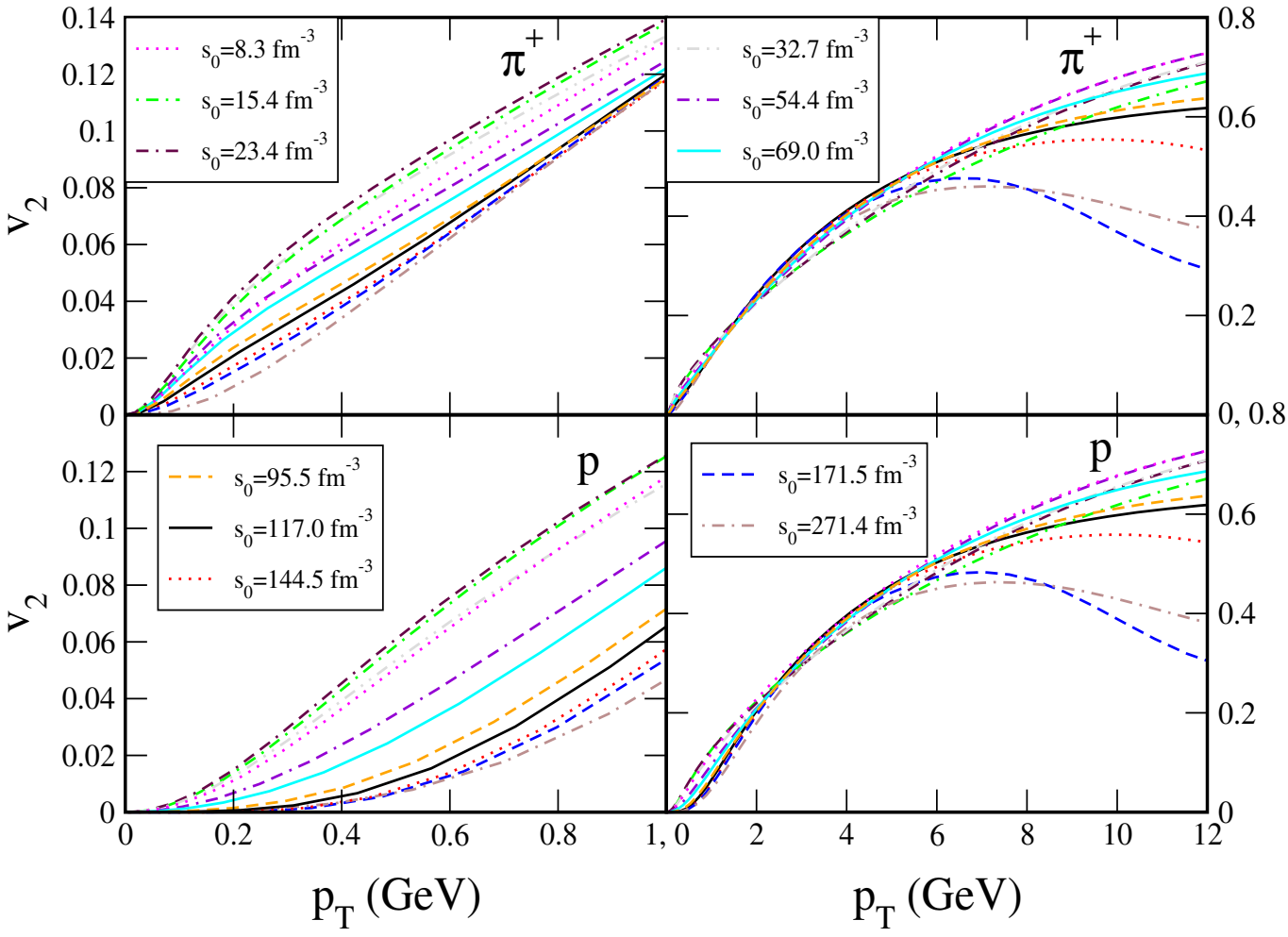

FIG. 8: Differential elliptic flow for thermal protons and π^+ as a function of transverse momentum for $b = 7\,\mathrm{fm}$ Au+Au collisions with various initial peak entropy densities s_0.

In Figure 8 we look at differential elliptic flow for both protons and π^+ as a function of transverse momentum for $b = 7\,\mathrm{fm}$ Au+Au collisions with various energies. The left panels are expanded views

of the low-p_T end; at all collision energies, over 99 percent of all particles are emitted with transverse momenta below 1.5 GeV. For this reason it is important to focus on the system's characteristics in more detail at low p_T. At low transverse momentum we notice that for both protons and π^+ the differential elliptic flow is not monotonic with collision energy. For the set of lowest energy collisions the differential elliptic flow seems to increase with $\sqrt{s}$, but then at all collisions with $\sqrt{s} \geq 10\,\mathrm{GeV}$ the differential elliptic flow decreases with increasing collision energy (see solid red line in the lower panel of Figure 10). This decrease in differential elliptic flow with increasing collision energy is due to the increase in radial flow for higher energy collisions. At lower collision energies $\sqrt{s} < 5\,\mathrm{GeV}$, the hydrodynamic expansion is cut short by kinetic freeze-out before the momentum anisotropy fully develops. For this reason, v_2 decreases as the collision energy is further reduced, both at fixed p_T and integrated over transverse momentum (see upper panel in Figure 10). The net result is the non-monotonic $\sqrt{s}$-dependence of v_2 seen in Figure 10, first predicted in [14].

While the total (p_T-integrated) pion elliptic flow increases from RHIC to LHC by about 25% [12], very little of this increase ($\sim 5\%$) is of ideal fluid dynamical origin, most of it stemming from the *disappearance* of late hadronic viscous effects between RHIC and LHC. At fixed p_T Figure 9 shows a *decrease* of v_2, reflecting a shift of the momentum anisotropy to larger p_T by increased radial flow, which flattens the LHC p_T-spectra, affecting the heavier protons more than the lighter pions (see Figure 6, right column). These radial flow effects on $v_2(p_T)$ are very small for pions but clearly visible for protons.

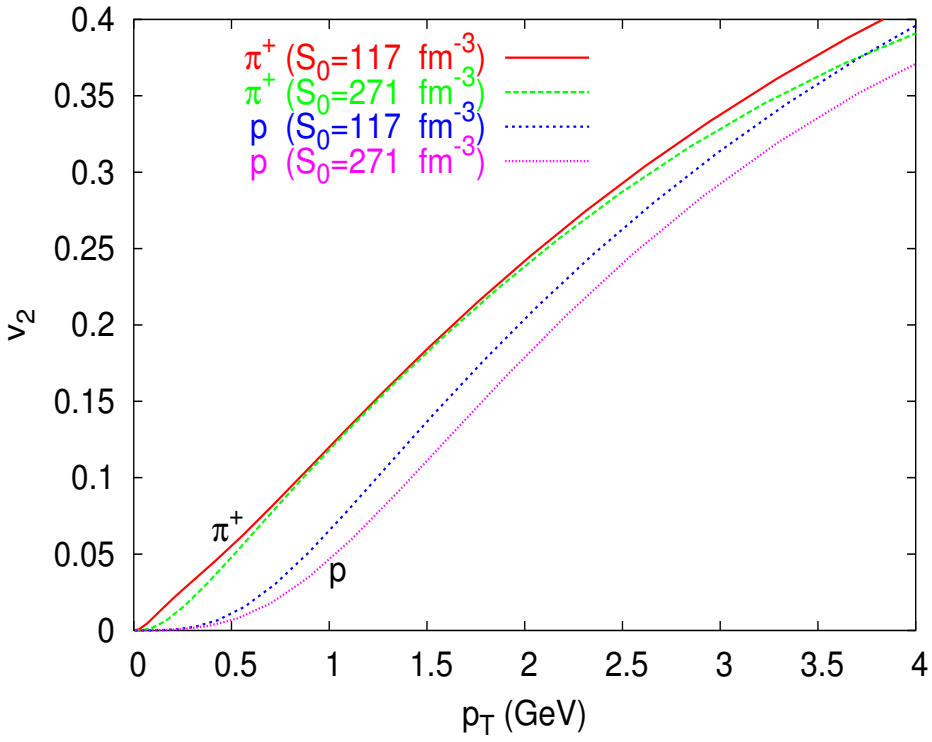

FIG. 9: Differential elliptic flow for protons and π^+ from $b = 7\,\mathrm{fm}$ Au+Au collisions at RHIC ($s_0 = 117\,\mathrm{fm}^{-3}$) and LHC ($s_0 = 271\,\mathrm{fm}^{-3}$) energies as a function of transverse momentum, plotted together for comparison.

The top panel of Figure 10 shows the p_T-integrated π^+ elliptic flow as a function of collision energy for $b = 7\,\mathrm{fm}$ Au+Au collisions. Shown is the p_T-integrated elliptic flow for thermally emitted pions (dashed line) as well as (solid line) for all pions (including thermally emitted pions and pions arising from the decay of unstable hadronic resonances after freeze-out). The peak in both these curves corresponds to the onset of the QGP phase transition below which the ideal hydrodynamic

prediction breaks down. Due to this breakdown, this peak is not observed in the experimental data [15]; instead, the measured elliptic flow decreases monotonously with decreasing collision energy.

Above RHIC energies, the ideal fluid dynamical model so far shows all signs of being reliable. Both curves in the upper panel of Figure 10 show an increase of the elliptic flow from RHIC to LHC. While the differential elliptic flow (as revealed in Figure 8) decreases at low p_T going from RHIC to LHC, the p_T-integrated elliptic flow increases from RHIC to LHC, because of radial flow: Radial flow flattens the LHC spectra dramatically, putting a larger weight on the larger v_2 values at higher p_T, and as a result the p_T-integrated elliptic flow is larger at LHC.

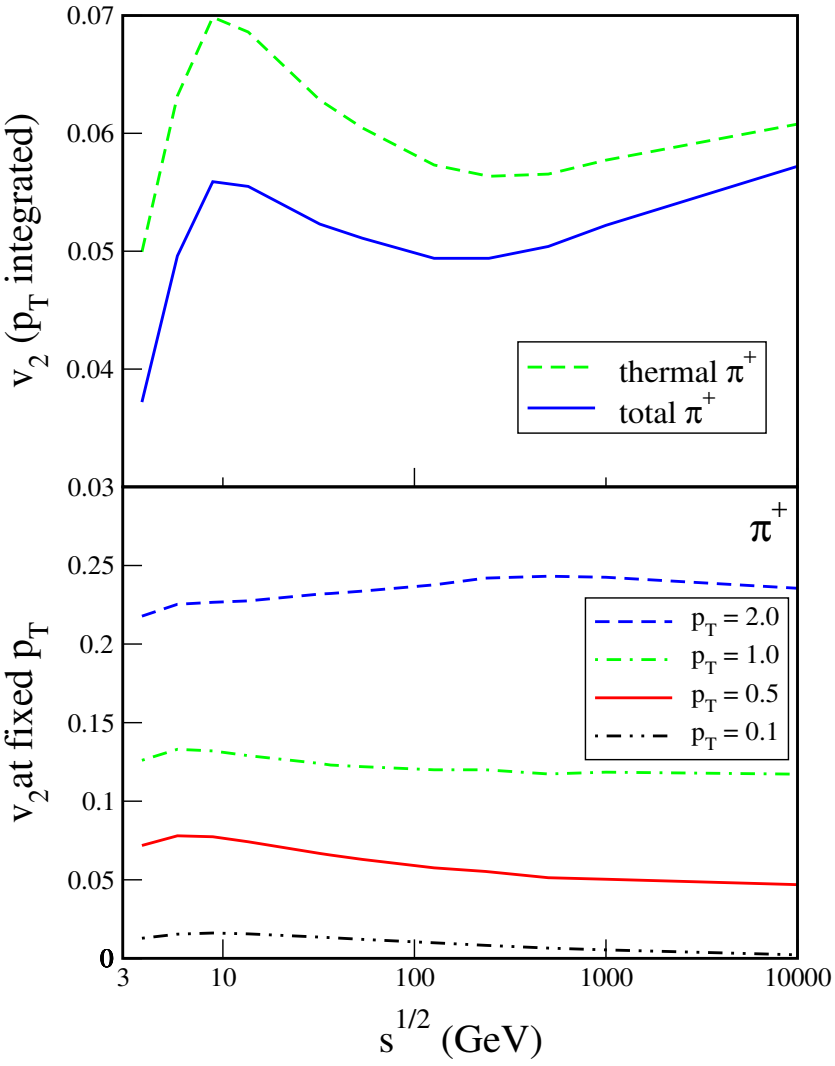

FIG. 10: Upper panel: Integrated π^+ elliptic flow as a function of collision energy for $b = 7$ fm Au+Au collisions (assuming the relation between s_0 and $\sqrt{s}$ shown in Figure 4). Lower panel: Elliptic flow at 3 fixed p_T values, shown as a function of collision energy, for $b = 7$ fm Au+Au collisions.

We should notice that at all collision energies the directly thermally emitted pions show more p_T-integrated elliptic flow than all pions together. From this we can deduce that pions emitted from resonance decays have a lower momentum anisotropy. This is at least partially understood by the fact that decay pions typically have smaller transverse momenta than their parent resonances [1].

The bottom panel of Figure 10 shows elliptic flow as a function of collision energy for various fixed transverse momenta. Looking at each of the lines individually, we see at low p_T the same non-monotonic $\sqrt{s}$ dependence as for the p_T-integrated elliptic flow in the upper panel. The continuous

decrease with rising $\sqrt{s}$ above $\sqrt{s} \sim 10\,\mathrm{GeV}$ of v_2 at fixed p_T differs from the increase of the integrated elliptic flow above $\sqrt{s} \sim 200\,\mathrm{GeV}$. This is a result of increased radial flow and spectra flattening that comes with the increase in $\sqrt{s}$. That is, radial flow causes more pions to be quickly moving outward with higher p_T in *all* directions, thus we have a lower elliptic flow at low p_T.

Conclusion

When experimental data will become available for very high energy collisions, comparison to these simulation results will provide insights into the validity of ideal hydrodynamics at high energy densities. Also, understanding the deviations from hydrodynamic predictions in low energy collisions will lead to more accurate dynamical models for the system of matter created in such collisions.

ACKNOWLEDGMENTS

We thank Rupa Chatterjee, Evan Froderman, Richard Furnstahl, and Huichao Song for their help. This work was supported by the National Science Foundation under grant PHY-0354916 and by the United States Department of Energy under the grant DE-FG02-01ER41190. Some of the results presented here were previously reported and published in Refs. [10, 16, 17].

[1] U. Heinz, *Concepts of Heavy-ion Physics*, Lecture Notes, arXiv:nucl-th/0407360 (2004).
[2] E. Schnedermann and U. Heinz, Phys. Rev. C **47**, 1738 (1992).
[3] P. F. Kolb and U. Heinz, in: *Quark-Gluon Plasma 3*, edited by R. C. Hwa and X.-N. Wang (Singapore: World Scientific 2003), p. 634 [nucl-th/0305084].
[4] http://nt3.phys.columbia.edu/people/molnard/OSCAR/ and references listed there.
[5] STAR Collaboration, Phys. Rev. Lett. **92**, 112301 (2004).
[6] F. Karsch and E. Laermann, *Thermodynamics and in-medium hadron properties from lattice QCD*, in *Quark Gluon Plasma 3*, edited by R. C. Hwa and X. N. Wang (World Scientific, Singapore, 2004), p. 1 [hep-lat/0305025].
[7] P. Braun-Munzinger, J. Stachel, C. Wetterich, Phys. Lett. B **596**, 61 (2004).
[8] PHOBOS Collaboration, Phys. Rev. C **74**, 021902(R) (2006).
[9] C. M. Hung and E. Shuryak, Phys. Rev. C **57**, 1891 (1998).
[10] N. Armesto *et al.* (incl. G. Kestin), J. Phys. G: Nucl. Part. Phys. **35**, 054001 (2008)
[11] T. Hirano *et al.*, Phys. Lett. B **636**, 299 (2006).
[12] T. Hirano *et al.*, J. Phys. G: Nucl. Part. Phys. **34**, S879 (2007).
[13] H. B. Meyer, Phys. Rev. D **76**, 101701 (2007).
[14] P. F. Kolb, J. Sollfrank and U. Heinz, Phys. Lett. B **459**, 667 (1999); and Phys. Rev. C **62**, 054909 (2000).
[15] U. Heinz, J. Phys. G: Nucl. Part. Phys. **31**, S717 (2005).
[16] U. Heinz and G. Kestin, PoS **CPOD2006**, 038 (2006) [arXiv:nucl-th/0612105].
[17] U. Heinz and G. Kestin, Eur. Phys. J. Spec. Top. **155**, 75 (2008) [arXiv:0709.3366 [nucl-th]].